Robotics and Computer Integrated Manufacturing 57 (2019) 496–505

Contents lists available at ScienceDirect

Robotics and Computer Integrated Manufacturing

journal homepage: www.elsevier.com/locate/rcim

Full length Article

Research and implementation of a non-supporting 3D printing method based on 5-axis dynamic slice algorithm

Wang Mingqian[a], Zhang Haiguang[a,b,c,*], Hu Qingxi[a,b,c,*], Liu Di[a], Lammer Herfried[d]

[a] Rapid Manufacturing Engineering Center, School of Mechatronical Engineering and Automation, Shanghai University, Shanghai 200444, China
[b] Shanghai Key Laboratory of Intelligent Manufacturing and Robotics, Shanghai University, Shanghai 200072, China
[c] National Demonstration Center for Experimental Engineering Training Education, Shanghai University, Shanghai 200444, China
[d] Kompetenzzentrum Holz GmbH, Altenberger Straße 69, 4040 Linz, Austria

ARTICLE INFO

Keywords:
3D printing
5-axis dynamic slicing
Non-supporting material printing (NSMP)
Skeleton extraction

ABSTRACT

Conventional three-dimensional (3D) printing technology generates objects and parts layer by layer by depositing material along the *Z*-axis direction. However, when it comes to overhanging structures in the printing process, the conventional printing process needs the creation of additional supporting structures. So, this technique requires additional materials and increases the effective printing time. To overcome these issues, this paper proposes a novel 5-axis dynamic slicing algorithm to achieve non-supporting material printing (NSMP). The original model is sliced by a series of dynamic planes calculated by the skeleton extraction; the 5-axis printing G-code generated from the sliced layers can control the 5-axis printer to complete NSMP. Finally, a comparison between traditional 3D printing and 5-axis printing is presented to test the utility of this strategy.

1. Introduction

A 30-year long development made the 3D printing technology become more and more mature. The 3D printing technology first described in 1986 by Charles Hull can fabricate any complex objects and become more and more popular in industrial application [1]. The 3D printing is based on layer-by-layer fabrication from an arbitrary geometric model to a real object. Due to the customized and arbitrary part production, 3D printing is widely applied in many industrial sectors, such as electronics [2], energy devices [3], medicines [4], biotechnology [5], optics [6], structural industry [7], automotive, and aerospace [8].

Nowadays, the 3D printing includes fused deposition modeling (FDM), stereolithography (SLA), selective laser sintering (SLS), powder bed with inkjet head 3D printing (3DP), and 3D plotting [9]. Especially, small-size printers and the widely open development sources made the FDM 3D printers become popular and affordable [10]. Those common printing strategies generate parts or structures adding the material layer by layer. Therefore, the overhangs structures in the object must be printed after building or pre-placed some supporting structures. Furthermore, the generation of the model with supporting structures requires more material, longer printing time and needs post-processing (for example, peeling off the supporting structures and cleaning or polishing the surface of the part).

Many strategies exist to achieve non-supporting material printing (NSMP). For example, Zhao et al. proposed that the overhang structure can be printed by inclined layer printing. This methodology can print overhang structures with a conventional 3D printer conveniently, however the nozzle is not perpendicular to the printing surface, and the underside of the cantilever structure is prone to burrs [11]. Wu et al. proposed the use of wire printing to print arbitrary meshes with 5 degrees of freedom (DOF) wireframe printer, and this method can realize the printing of surface contours of complex cantilever models [12]. The use of model auto-partitioning algorithm for generating three-dimensional layer information to build overhang/undercut features was proposed by Lee et al. The cantilever portion divides the original model, followed by slicing the divided sub-models separately [13]. For improving the flexibility of 3D printing generation process, Keating et al. proposed the use of a multi-functional robotic platform to print regular curved part and hollow cube [14]. Lee et al. proposed the use of model segmentation to generate a Γ-shaped component with a 5-axis FDM apparatus [15], while Wu et al. proposed the use of a 6-DOF robotic platform to generate the overhang structure according to the collision-free sequences determined by model segmentation for NSMP [16].

These existing printing methods can achieve NSMP to some extent, all focusing on the outer contour of the solid model without printing the support. However, achieve NSMP for overhang structures with internal continuous holes or grooves is not easy because, in such cases, the

* Corresponding authors.
E-mail addresses: haiguang_zhang@i.shu.edu.cn (H. Zhang), huqingxi@shu.edu.cn (Q. Hu).

https://doi.org/10.1016/j.rcim.2019.01.007
Received 29 May 2018; Received in revised form 11 January 2019; Accepted 11 January 2019
Available online 18 January 2019

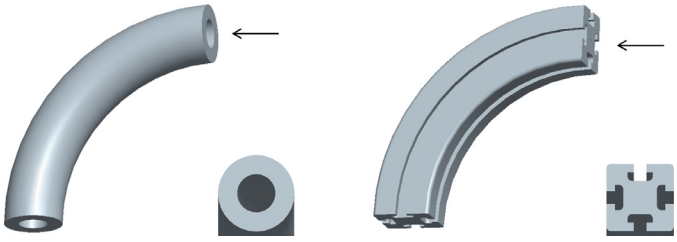

Fig. 1. Regular arc with cantilever structure with holes or slots.

removal of the additional support structure is difficult. This study mainly focuses on the NSMP of a cantilevered structure with continuous holes or grooves, while avoiding the external and internal support structure of the overhang structure in printing mechanism, reducing the printing consumables and time, avoiding the post-treatment process of peeling off the support materials, and improving the flexibility of non-supporting printing process. The proposed technology can be applied to the production of hydraulic or pneumatic piping structures, cooling systems, chemical pharmaceutical microfluidic feed integrated systems, and the manufacture of complex components or connectors.

2. 5-axis printing methodology

2.1. 5-axis printing overview

The above problems mainly apply to the FDM printing of an unsupported structure with internal holes or slotted cantilever structures. This study focuses on regular curved pipes with circular through-holes and arcs with T-shaped slots on the outside (see Fig. 1). These two typical models can be used for connectors in special engineering applications.

The cantilever structure model inevitably generates a support structure during normal 3D printing. The model is imported in Repetier-Host software using the conventional 3D print Cura slicing engine for the slicing (see Fig. 2). In Fig. 2, the blue part is the cantilever printed model part, and the orange part is the printed support

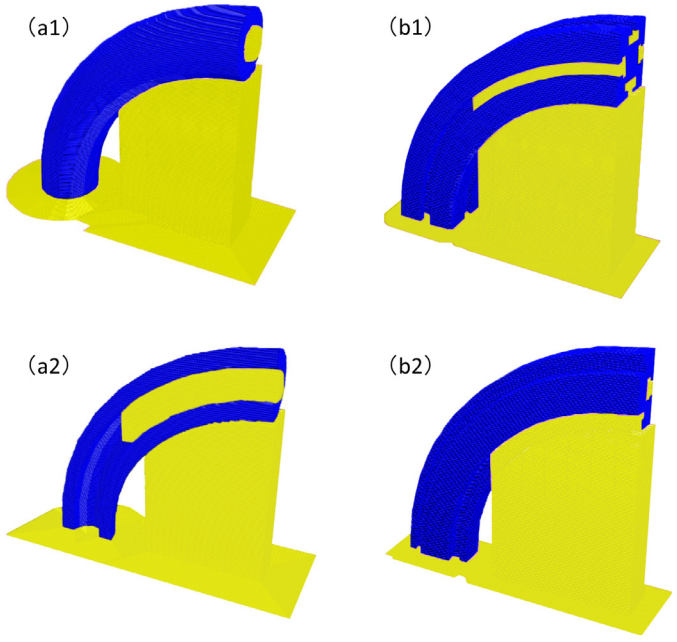

Fig. 2. Support for 3D slicing process of cantilever structures with regular arcs and holes or slots; (a1) Support structure for elbow models; (a2) Support structure for elbow cut model; (b1) Structure of the model; (b2) Support structure of curved I-section model.

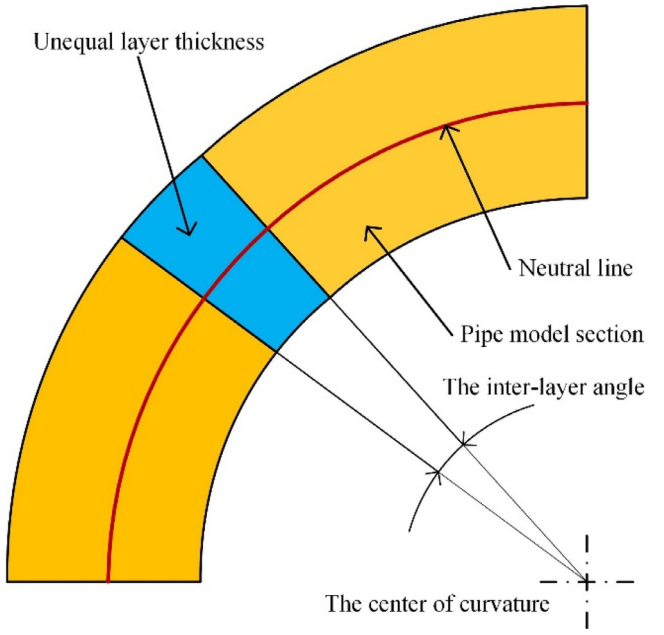

Fig. 3. The unequal layer thickness problem.

part. After the slicing, the printing process consumes material more than twice that used for the cantilever model body, and the supporting material in both the arc-shaped models is difficult to peel off. Even if the supporting material can be peeled off, the peeling device easily scratches the surface of the print, and the removal requires great physical strength and time. The parts, in this specific case, can be easily generated by multi-axis composite printing without the support. In the slicing process, the slice plane should be dynamically adjusted in real time according to the freedom of multiple axes.

In the 5-axis dynamic slicing process, a real-time dynamic adjustment of the slice plane results in non-parallel planes between the layers, thus leading to a non-uniform thickness between layers. In Fig. 3, the blue part is the single-layer printing layer thickness, the orange area is the model with a central skeleton curve, and the red line is the central curve. The thickness of the printed layer is related to the distance between the layers and the distance from the midpoint of the layer to the center of the curvature. Inter-layer printing is generally a continuous line segment printing. To improve the accuracy and the overall print quality of the model, a continuous line segment is subdivided into many small line segments, and then the extrusion thickness of each line segment is calculated by the distance from the midline point of each line segment to the center point of curvature.

For this kind of model with a particular neutral trajectory feature, the curve skeleton can be extracted from the point cloud data composed of the nodes on the STL model triangle patch [17], the spatial 5-axis dynamic slice of cantilever structure model realize by the curve skeleton, and the layer thickness can be calculated between the slices.

2.2. 5-axis dynamic slicing algorithm

Fig. 4 shows the 5-axis slicing algorithm to deal with a hole or slot cantilever structure. The commercial software Pro/E 5.0 was used to design the cantilever structure model and export the STL file. Then, a program in a python script was written to read the triangular slices in the STL file and save it in the computer's cache with the data structure of the list.

2.2.1. Skeleton extraction

Fig. 5 represents the skeleton curve extraction process of a spiral-shaped cantilever structure model. The extraction of the skeleton is

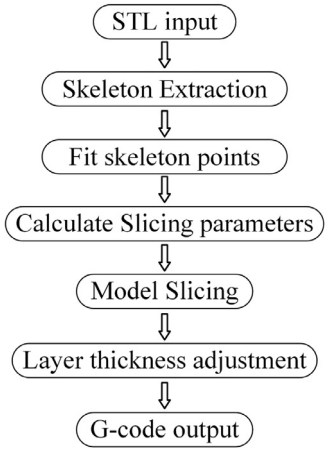

Fig. 4. 5-axis print slicing algorithm.

suitable for the most of models, and the model skeleton [18] is implemented using the mean curvature flow algorithm (MCF). Here, the spring model is used as an example to show the extraction process. Pro/E software is used to design the target model which is further exported as an STL file format. The STL model file is extracted as a point cloud model file. Then the skeleton point set of the model is extracted using the MCF algorithm, and the skeleton point set is fitted with a space curve to obtain a neutral curve of the model.

2.2.2. Fitting the skeleton points

This paper fits the neutral skeleton point set using the Bezier spline curves [19]. Assume that $n+1$ control point positions are given: $\boldsymbol{p}_k = (x_k, y_k, z_k)$, where k can take any integer values from 0 to n. These coordinate points will be mixed to produce the position vector $\boldsymbol{P}(u)$, which is used to describe the path of the approximation of the Bezier polynomial function between $\boldsymbol{p}_0$ and $\boldsymbol{p}_n$.

The position vector $\boldsymbol{P}(u)$ can be represented by the cured function:

$$\boldsymbol{P}(u) = \sum_{k=0}^{n} \boldsymbol{p}_k BEZ_{k,n}(u), \quad 0 \le u \le 1 \tag{1}$$

$BEZ_{k,n}(u)$ is Bezier mixed function and is the Bernstein polynomial given by

$$BEZ_{k,n}(u) = C(n, k)u^k(1-u)^{n-k} \tag{2}$$

where parameter function $C(n, k)$ is the binomial coefficient

$$C(n, k) = \frac{n!}{k!(n-k)!} \tag{3}$$

The vector equation represents the set of three parametric equations for a single curve coordinate.

$$\begin{cases} x(u) = \sum_{k=0}^{n} x_k BEZ_{k,n}(u) \\ y(u) = \sum_{k=0}^{n} y_k BEZ_{k,n}(u) \quad 0 \le u \le 1 \\ z(u) = \sum_{k=0}^{n} z_k BEZ_{k,n}(u) \end{cases} \tag{4}$$

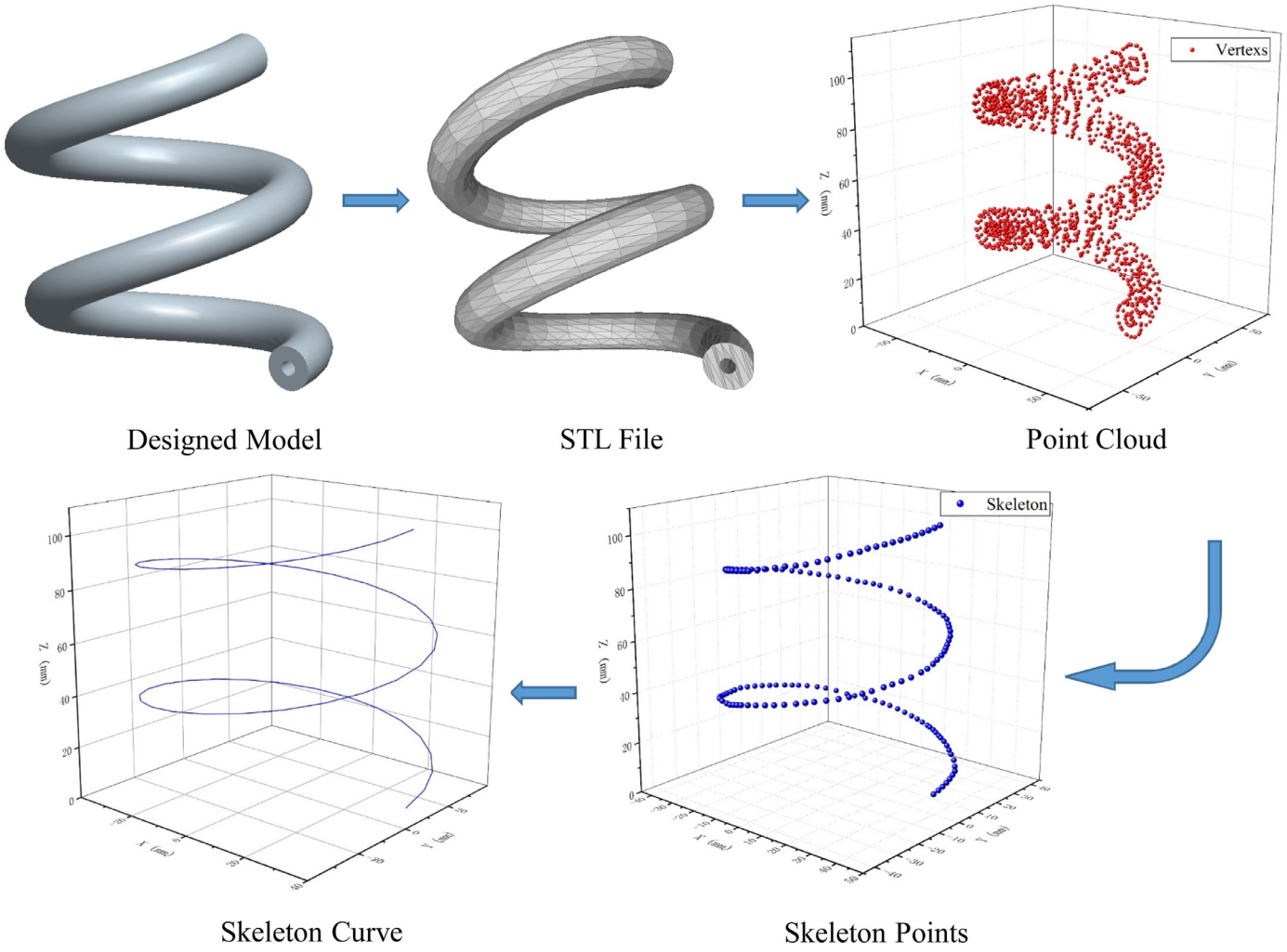

Fig. 5. Skeleton curve extraction process.

Consecutive binomial coefficients can be obtained using recursive calculations:

$$C(n, k) = \frac{n-k+1}{k} C(n, k-1) \tag{5}$$

When $n \geq k$, Bezier mixed functions also conform to recursive relations:

$$BEZ_{k,n}(u) = (1-u)BEZ_{k,n-1}(u) + uBEZ_{k-1,n-1}(u), \quad n > k \geq 1 \tag{6}$$

In that case $BEZ_{k,k} = u^k$ and $BEZ_{0,k} = (1-u)^k$. The skeleton points obtained by the contracting model point cloud data are then fitted into Bezier spline curves $\boldsymbol{P}(u)$.

2.2.3. Calculation of slicing parameters

The layer thickness should be provided to calculate the whole numbers of slices, and each point of the slice and Bezier spline curves can be calculated by the differential curved length and the integral curved length. The differential curved length, given by:

$$ds = \sqrt{dx^2 + dy^2 + dz^2}\, du = \sqrt{x'(u)^2 + y'(u)^2 + z'(u)^2}\, du \tag{7}$$

Using the fitted neutral curve arc length to represent the 5-axis composite printed stack thickness scalar, the Bezier spline curve arc length integral is calculated as follows:

$$S(u) = \int_0^u \sqrt{x'(u)^2 + y'(u)^2 + z'(u)^2}\, du = it = s \tag{8}$$

where i is slice layers number ($0 \leq i \leq maxNums$), and the maximum of i is given by:

$$\max Nums = \frac{1}{t} \int_0^1 \sqrt{x'(u)^2 + y'(u)^2 + z'(u)^2}\, du \tag{9}$$

t is slice layer thickness, which is approximately equal to the arc length as the slice accuracy parameter.

Next, find the slicing point of the slicing neutral layer and the tangent of the point location.

From Eq. (8), $S(u) = \int_0^u \sqrt{x'(u)^2 + y'(u)^2 + z'(u)^2}\, du = it$, and the current point relative parameters u can be calculated as $u_c = f(i, t)$. In that case, the intersection of the current slice and the neutral curve is $\boldsymbol{P_C} = (x(u_c),\ y(u_c),\ z(u_c))$, and the tangent vector at this point is $\boldsymbol{\tau_c} = \boldsymbol{P}(u)' = (x'(u_c),\ y'(u_c),\ z'(u_c))$.

The coordinates of the intersection point of each slice and the intersection tangent vector data of the fitted Bezier spline curve are calculated; these data are constructed as a slice driving parameter object, and the slice driving parameter object of each layer is stored as a list data structure.

Assuming the traversal point is $\boldsymbol{P_C}$, traverse the list of slicing-driven parameter objects. When printing to $\boldsymbol{P_C}$ point location, according to the existing equipment, the direction of the nozzle should be along the direction of the point of the vector to ensure that the nozzle is always in the vertical direction. The cantilever model triangle list and printing points $\boldsymbol{P_C}$ are accompanied by the rotation of the platform. As Fig. 6 shows, the diagram illustrates the positional relationship between the print head and the printed dot direction vector. Using the tangent vector of intersection point $\boldsymbol{P_C}$, the rotation angle of the A-axis and C-axis in the 5-axis printing is determined. The A-axis rotation angle is $\theta = arccos\frac{z'(u_c)}{|\boldsymbol{P}(u)'|}$, while that of C-axis $\delta = arctan\frac{y'(u_c)}{x'(u_c)}$.

2.2.4. Model slicing

When the A-axis and C-axis are rotated, the spatial position transformation matrix is needed to dynamically transform the spatial position of the cantilever structure model and the intersection point of the current slice and neutral curve.

The transformation matrix is given by:

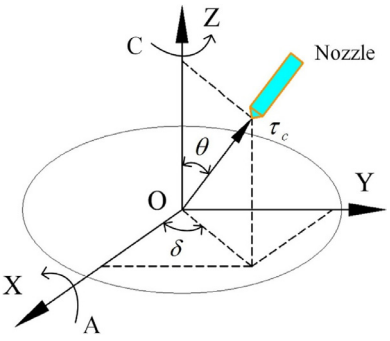

Fig. 6. 5-axis printing: A-axis and C-axis.

$$\boldsymbol{T} = \boldsymbol{Tran_b} \cdot \boldsymbol{Rot} \cdot \boldsymbol{Tran_a} \tag{10}$$

In the workpiece coordinate system of the receiving platform, due to the specific structural design, in more than a case the receiving platform and the rotation axis are not coplanar. In this study, the axes of the A-axis and the receiving platform have a positional offset, and the rotation of the model is in the process. Rotate the model along the intersection point A of the A-axis and the C-axis, and then rotate the model to the position of point R. The translation matrix $\boldsymbol{Tran_b}$ is:

$$\boldsymbol{Tran_b} = \begin{bmatrix} 1 & 0 & 0 & -x_R \\ 0 & 1 & 0 & -y_R \\ 0 & 0 & 1 & -z_R \\ 0 & 0 & 0 & 1 \end{bmatrix} \tag{11}$$

The rotation matrix around the A- and C-axes is:

$$\boldsymbol{Rot} = \boldsymbol{Rot}(\boldsymbol{A}) \cdot \boldsymbol{Rot}(\boldsymbol{C}) = \begin{bmatrix} 1 & 0 & 0 & 0 \\ 0 & cos\theta & -sin\theta & 0 \\ 0 & sin\theta & cos\theta & 0 \\ 0 & 0 & 0 & 1 \end{bmatrix} \cdot \begin{bmatrix} cos\delta & -sin\delta & 0 & 0 \\ sin\delta & cos\delta & 0 & 0 \\ 0 & 0 & 1 & 0 \\ 0 & 0 & 0 & 1 \end{bmatrix} \tag{12}$$

After the model rotates around point R, the model needs to be translated again to the origin of the workpiece coordinate system. That is, if the model needs to be reattached to the surface of the print receiving platform, an inverse translation transformation is required:

$$\boldsymbol{Tran_a} = \begin{bmatrix} 1 & 0 & 0 & -x_R \\ 0 & 1 & 0 & -y_R \\ 0 & 0 & 1 & -z_R \\ 0 & 0 & 0 & 1 \end{bmatrix} \tag{13}$$

Fig. 7 shows the schematic diagram before and after the transformation of all STL vertexes and the printing point $\boldsymbol{P_C}$ of the slice. Before slicing the normal plane where the point $\boldsymbol{P_C}$ is located, the model needs to be transformed, and the current printing point $\boldsymbol{P_C}$ is transformed by matrix($\boldsymbol{P_{CT}} = \boldsymbol{T} \cdot \boldsymbol{P_C}$). When the rotation of the platform satisfies the vertical direction (i.e., the direction of the nozzle) of the printing point, $\boldsymbol{P_C}$ and the vertex of the nozzle lie on the same horizontal plane. At this

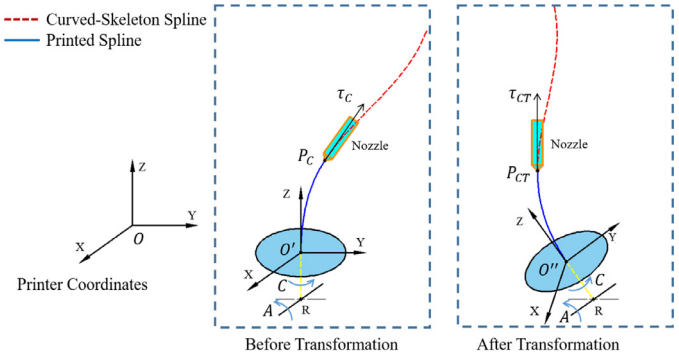

Fig. 7. 5-axis print slice space transformation map.

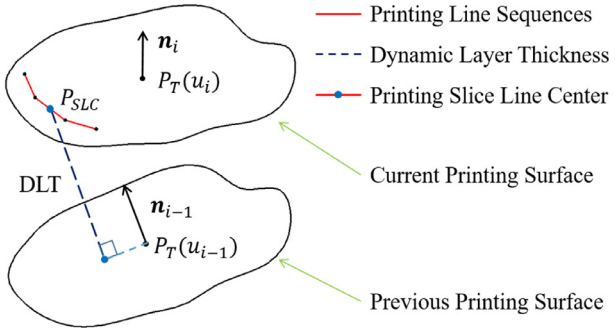

Fig. 8. The schematic 5-axis printing slice dynamic layer thickness adjustment.

time, the rotated cantilever STL structure is sliced along the Z coordinate plane of the transformed printing point $\boldsymbol{P_C}$.

2.2.5. Layer thickness adjustment

After slicing, the list of contour segments of the model slice can be got. Filling the inside of the outline to get the filled line segment clusters, the contour line clusters and the fill line segment clusters are the objects that generate the printing G-code, and they can be combined into a print line segment cluster. Section "five-axis printing overview" states that the 5-axis dynamic slice have a non-uniform layer thickness, and each thread segment in the print line segment is dynamically adjusted for the thickness of the pultruded thread.

From Fig. 8, because in the 5-axis print slicing process two adjacent slicing levels determine the squeezing thickness of extruder when printing a certain slicing line segment sequence, the middle point of the printable line segment $\boldsymbol{P_{SLC}} = (x_{SLC}, y_{SLC}, z_{SLC})$ was executed to calculate the layer thickness. Since the position of the spray head is always in the vertical direction, the current print layer plane is in a horizontal position and its normal vector $\boldsymbol{n_i} = (0, 0, 1)$. However, the previous slice plane always changes the spatial position with the rotation of A- and C-axes. After transformation, the normal vector of the previous print plane is $\boldsymbol{n_{i-1}} = \boldsymbol{T}\cdot\boldsymbol{n_i} = (x_n, y_n, z_n)$. Meanwhile, the previous intersection of the current slice and the neutral curve is $\boldsymbol{P_T}(\boldsymbol{u_{i-1}}) = (x(u_{i-1}), y(u_{i-1}), z(u_{i-1}))$. Afterwards, the plane equation of previous printing plane can be obtained from the intercept point and the normal vector of the plane, and the previous slice plane can be shown as below:

$$\boldsymbol{S}: x_n(x - x(u_{i-1})) + y_n(y - y(u_{i-1})) + z_n(z - z(u_{i-1})) = 0 \tag{14}$$

The previous slice plane can be simplified into the general form of the plane equation:

$$\boldsymbol{S}: x_n x + y_n y + z_n z - x_n x(u_{i-1}) - y_n y(u_{i-1}) - z_n z(u_{i-1}) = 0 \tag{15}$$

Calculate the thickness of printed line. Due to the unequal layer thickness of each printed line, each printed line layer thickness can be defined as the dynamic layer thickness (DLT):

$$DLT = \frac{|x_n x_{SLC} + y_n y_{SLC} + z_n z_{SLC} - x_n x(u_{i-1}) - y_n y(u_{i-1}) - z_n z(u_{i-1})|}{\sqrt{x_n^2 + y_n^2 + z_n^2}} \tag{16}$$

The calculated DLT of the segment thickness of each segment is added to the line segment attribute, the print line segment object is reconstructed, and the print line segment cluster is saved in the slice layer list.

2.2.6. G-code output

Continue to traverse the slicing drive parameter list, and repeat the above slicing operation until the slicing drive parameter list is traversed and a complete slice layer list is finally obtained.

Then, the slice layer list is iterated to obtain the point coordinates of each print line segment $\boldsymbol{P_0}$ and $\boldsymbol{P_1}$. Note that the class definition of print line segment in the computer is composed of the parameters of starting point $\boldsymbol{P_0}$ and ending point $\boldsymbol{P_1}$. Because the workpiece coordinate system of the receiving platform and the device origin coordinate system are not coincident, a translation matrix transformation is needed to convert the sliced print line segment coordinate into a coordinate in the printer coordinate system to achieve a specific print position control. The coordinate system transformation matrix is given by:

$$\boldsymbol{Tran_c} = \begin{bmatrix} 1 & 0 & 0 & x_c \\ 0 & 1 & 0 & y_c \\ 0 & 0 & 1 & z_c \\ 0 & 0 & 0 & 1 \end{bmatrix} \tag{17}$$

Therefore, each point of the output G-code relative to the printer coordinates is: $\boldsymbol{P_{M0}} = \boldsymbol{Tran_c}\cdot\boldsymbol{P_0}$, $\boldsymbol{P_{M1}} = \boldsymbol{Tran_c}\cdot\boldsymbol{P_1}$. Print segments $\boldsymbol{P_{M0}P_{M1}}$ based on the relative printer coordinate system generate the 5-axis printing G-code.

2.3. 5-axis dynamic generation system

As shown in Fig. 9, the 5-axis dynamic generation system includes host system and lower computer control system. The host system can complete the overhang structure slicing mission including STL input, skeleton extraction, fitting skeleton points, calculation of slice

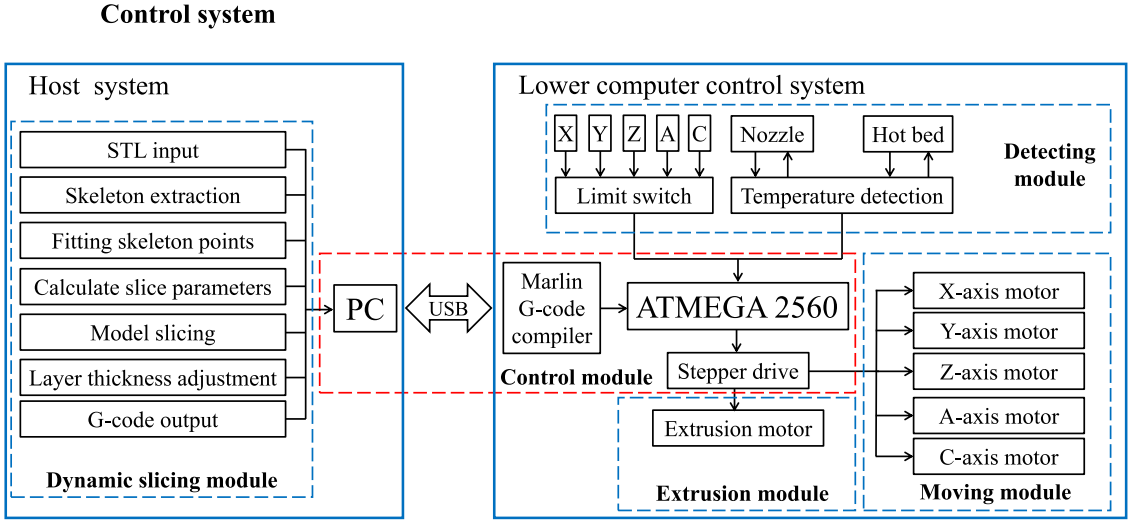

Fig. 9. 5-axis dynamic generation system.

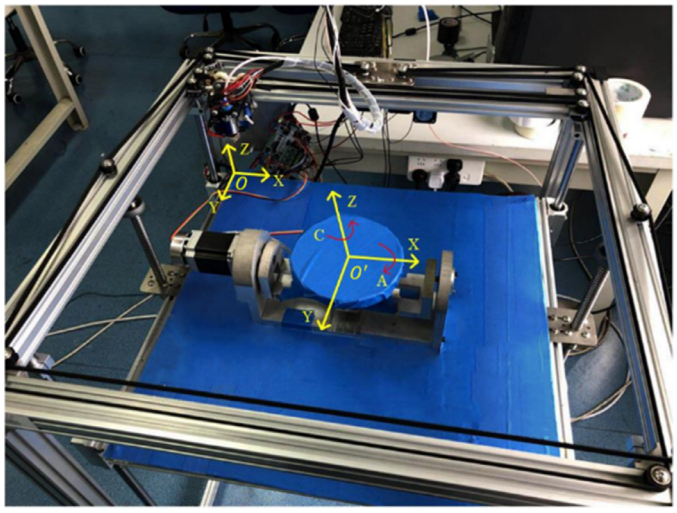

Fig. 10. The 5-axis printer.

parameters, model slicing, layer thickness adjustment and G-code output. The lower computer control system can execute the G-code from the host system and send the print status report to the host system through an USB communication. The lower computer control system includes control module, detecting module, extrusion module, and moving module. The control module includes the Marlin G-code compiler, ATMEGA 2560 (the high-performance, low-power Microchip 8-bit AVR RISC-based microcontroller) and stepper drive. Meanwhile, ATMEGA 2560 is also called micro controller unit (MCU). After Marlin completes the translation of G-code, it sends a command message to the MCU which in turn sends a motor command signal to the stepper drive to make the moving module to finish the relative movement and filament extrusion function. The detecting module ensures the machine coordinate system and the suitable printing temperature.

2.3.1. Machine and hardware

The 5-axis FDM printer was developed in our lab. Fig. 10 shows the printer structure. The device is composed of a frame whose overall size is of 740 × 740 × 1053 mm (LxWxH), with a 500 × 500 × 600 mm movable range of nozzle. The diameter of the printing adhesion surface of the receiving platform is 220 mm, the rotation range of the receiving platform (*A*-axis) is ± axi, the receiving platform (*C*-axis) can rotate freely, the *X*- and *Y*-axis movement accuracy of the printer is 0.01 mm, while that of *Z*-axis is 0.005 mm. Rotation accuracies of A- and *C*-axes are both 0.028°

The printer platform uses the ATMEGA 2560 as the master control chip of the equipment lower position machine, and through the Marlin Rumba series firmware communicates with the upper computer to realize multi-axis printing.

2.3.2. Software usage

The cantilever structure model was designed using Pro/E 5.0 commercial software, and the space-based 5-axis slicing program for cantilever structure model was written using Python 3.6; the 5-axis printing G-code generation was realized. The lower computer uses Arduino 1.8.5 open source software to develop the control of the seven motors of the printer (one motor for each of the *X*- and *Y*-axes, two motors for the *Z*-axis, one motor for the *A*-axis, one motor for the *C*-axis, and one for the extruded filament motor). The host computer adopts Repetier-Host V2.0.5 software to load the G-code into the software and communicates with the lower computer through the G-code to control the 5-axis printer.

3. Results and discussion

The 5-axis NSMP of several types of cantilever structures using the above method is compared to conventional in the slicing algorithm, the characteristics of printing process and the printed surface features.

3.1. Comparison of slicing algorithms

The three-dimensional slice algorithm mainly uses equidistant parallel planes for slicing the three-dimensional model to obtain outline information of the printed layer (Fig. 11). However, for the cantilever structure, the three-dimensional slice needs to automatically fill the support structure under the overhang portion of the original model and merge the original model and the support structure. Afterwards, they are sliced together, so that each structure layer includes the original model and support structure [20].

In the 5-axis slicing algorithm of this study, the skeleton of the model was extracted to find the printed slice point and normal plane as the slice plane and then calculates the print plane information where the normal plane and the cantilever model intersect. However, the layer thickness of each layer is not uniform and needs to be calculated during the slicing process so that the dynamic adjustment of the printing layer thickness can be achieved during the actual printing process.

Since the 5-axis slicing algorithm and the conventional slicing algorithm proposed in this study have essential differences, using the slicing algorithm and the typical Cura Engine slicing algorithm, the slicing time-consuming and output file temporary memory are compared.

According to Table 1, the number of slice layers, slice time, and

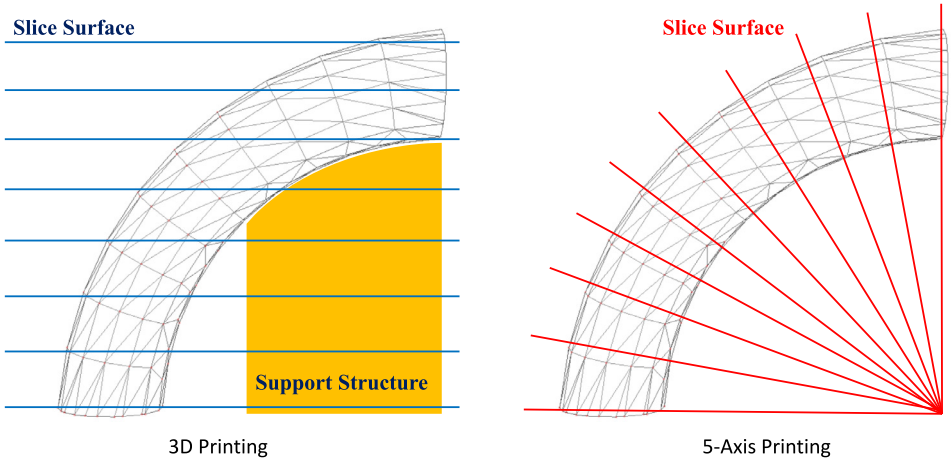

Fig. 11. Cantilever structure models with equal curvature.

Table 1
Comparison results of slicing effect.

Model name	Number of triangles	Slice thickness mm	Slice layers			Slice time (s)			Output file memory (kB)		
			Cura	5-Axis	Increase ratio	Cura	5-Axis	Increase ratio	Cura	5-Axis	Increase ratio
Hollow curved pipe		0.1	582	785	34.88%	4.78	6.67	39.54%	6043	7103	17.54%
	598	0.2	292	393	34.59%	2.61	3.24	24.14%	3032	3553	17.18%
		0.3	196	262	33.67%	1.76	2.31	31.25%	2041	2354	15.34%
T-slot curved rod		0.1	582	785	34.88%	6.48	10.17	56.94%	8168	12260	50.10%
	1308	0.2	292	393	34.59%	3.48	4.81	38.22%	4093	6139	49.99%
		0.3	197	262	32.99%	2.56	3.78	47.66%	2744	4144	51.02%
Spiral pipe	2738	0.1	1148	3958	244.77%	40.18	92.37	129.89%	43337	94400	117.83%
		0.2	575	1980	244.35%	20.26	45.58	124.98%	21716	48074	121.38%
		0.3	385	1320	242.86%	13.76	31.92	131.98%	14557	32581	123.82%

output file memory of the 5-axis model dynamic slice is larger than that of the conventional 3D printed slice, mainly because the 5-axes have more spatial transformations of the *A*-axis and the *C*-axis than the three axes and the corresponding Printer motor control. From 3-axis to 5-axis processes, the difficulty of spatial slices in relation to horizontal planar slices has increased by two dimensions. The higher the complexity of the model, the larger the number of slice layers and the more slice time, the more code memory the slices generate.

3.2. Printing process characteristics analysis

As shown in Fig. 12, the printing experiment uses a degradable natural thermoplastic PLA; the 3-axis printing uses gray wire while the 5-axis printing uses red wire; different colors allow to distinguish between different printing strategies. Fig. 12(a1) is a general 3D print of a cantilever structure with a T-slot, Fig. 12(a2) is a generic 3D print of a cantilever structure with a through hole, and Fig. 12(b1) is a 5-axis printer with a T-slot cantilever structure. Fig. 12(b2) shows a through-hole cantilever structure generated from a 5-axis printer, and Fig. 12(c) is a spiral-shaped pipe generated. Given the three structural models in the 3-axis printing and the 5-axis printing process, they can easily be printed with the same placement.

In a conventional 3D printing process, the forming direction of the model is always stacked layer by layer from bottom to top along the *Z*-axis direction, so the support structure may appear in the printable cantilever structure (see Fig. 12(a1) and (a2)). The printable cantilever structure requires a sufficient amount of support material to facilitate the forming, and the inner hole and outer groove of the cantilever structure are filled with the supporting material that is difficult to be peeled off during post-processing. As Fig. 12(b1), (b2) and (c) show, these cantilever structures are all implemented using 5-axis dynamic printing methods. These cantilever structures do not contain supporting materials after the inner hole and the outer groove are printed. No post-processing is required to remove the support structure. The 5-axis dynamic printing and ordinary 3D printing process printing process parameters can be shown in Table 2.

According to Table 2, the 5-axis dynamic printing process can avoid supporting materials to a greater extent than conventional 3D printing. For the cantilever structures of the hollow arc tube and the T-slot arc-shaped rod, the initial printing plane can be directly located on the printing platform, so this type of structure does not require any supporting material in the 5-axis dynamic printing process. For the space spiral tube model, the nozzle can easily interfere with the platform in the printing process, the receiving plane cannot be close to the printing plane, so a printing base is needed to provide the initial acceptance plane for the hollow spiral tube. Moreover, the 5-axis dynamic printing requires much lower amount of additional materials for generate objects than conventional 3D printing, the printing process is faster, and the printing efficiency is significantly improved. Compared to the conventional 3D printing, the 5-axis dynamic printing can save about 30.62%–60.61% materials and about 32.35%–48.87% time.

3.2. Printed surface features analysis

Fig. 13 is the real generation effect chart of cantilever models in conventional 3D printing. When the overhang angle of the cantilever model exceeds 45°, the printed part needs supporting materials for the complete shaping. With the layer-by-layer accumulation, the staircase effect on printed parts becomes more and more obvious because the stacking direction is not along the model's central skeleton. The through

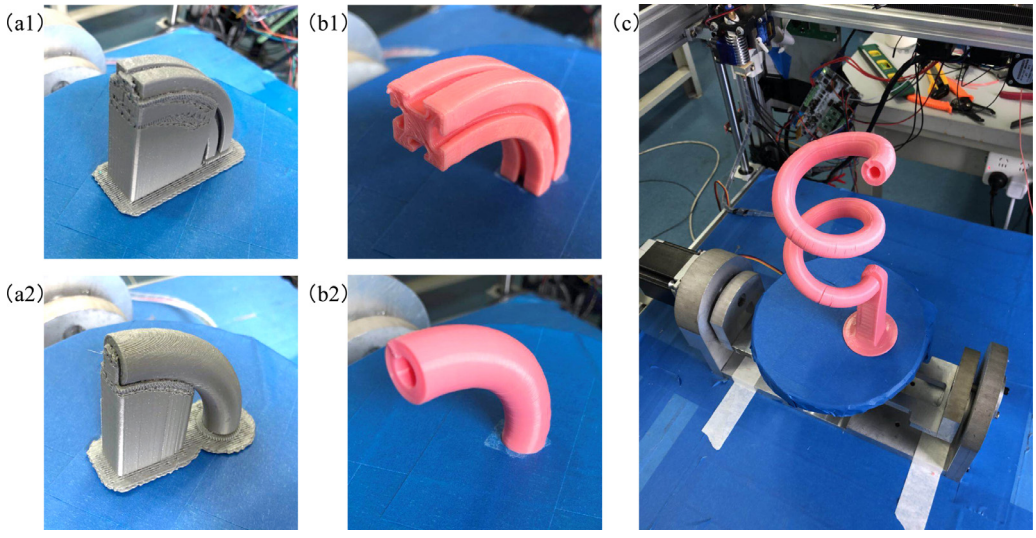

Fig. 12. Cantilever structure model printing.

Table 2
Comparison of printing process parameters.

Model name	Number of triangles	Slice thickness mm	Model material (g)		Support material (g)		Material saving rate (%)	Print time (h)		
			Cura	5-Axis	Cura	5-Axis		Cura	5-Axis	Reduce rate: (%)
Hollow curved pipe	598	0.1	14.63	15.24	5.29	NULL	31.99%	3.46	2.03	41.33%
		0.2	14.65	15.14	5.64	NULL	35.15%	2.52	1.52	39.68%
		0.3	14.64	13.54	5.40	NULL	44.40%	1.36	0.92	32.35%
T-slot curved rod	1308	0.1	17.83	22.95	6.58	NULL	30.62%	4.31	2.64	38.75%
		0.2	17.84	17.83	6.94	NULL	38.96%	2.93	1.98	32.42%
		0.3	17.83	12.72	6.69	NULL	38.14%	1.85	1.21	34.59%
Spiral pipe	2738	0.1	97.12	93.54	55.28	NULL	60.61%	26.03	13.31	48.87%
		0.2	97.14	98.79	56.25	NULL	56.21%	13.15	6.79	48.37%
		0.3	97.11	103.67	55.63	NULL	50.53%	9.51	5.32	44.06%

holes and side grooves of the cantilever print model contain support material which are difficult to be removed.

Fig. 14 shows a 5-axis dynamic printed part rendering. Fig. 14(a1) and (b1) are side views of the hollow arc tube and the T-slot arc rod, respectively, and the through holes and the through grooves at both ends can be clearly seen. The end faces of the hollow arc tube and the T-slot arc rod are shown in Fig. 14(a3) and (b3), and the through-hole and side-slot structure of the printing cantilever structure have good shape retention. Fig. 14(c1) is a hollow spiral tube print sample with internal permeability visible through the wire. Fig. 14(a2), (b2), and (c2) are front views of a hollow arc tube, a T-slot arc rod, and a spiral tube, respectively, while Fig. 14(a4), (b4), and (c3) are magnifications of the above printed parts. The melting of the cantilever structure is always along the tangent direction of the skeleton curve, and the layers have a good combination of surface ladder effect. However, due to the poor rigidity of the 5-axis printing platform, the vibration generated from the printing process of the cantilever model causes a local increase in the distance between a few layers on the surface of the model.

3.3. Discussion of 5-axis dynamic printing

This study mainly achieved NSMP of a space-based cantilever structure. As shown in Fig. 15, the 5-axis dynamic printing process of the cantilever structure converts the printing surface of each layer into a horizontal direction during printing to ensure that the printing head can be reached. However, due to the relatively poor rigidity of the 5-axis printing frame and the conventional 3D printing frame, vibration effects in the printing process are more obvious, and the rotation axis has a certain backlash that results in a large interval between some printed layers. As shown in Fig. 15(c2), the spiral print has two distinct printed segments with significant interlayer spacing.

For the hollow curved pipe and the T-slot curved rod structure (Fig. 16(a) and (b)), the initial acceptance planes for these types of cantilever structures can be located on the print hot bed platform, and thus can be achieved completely. However, for the spiral tube structure, if the end of the model is in the hot bed plane, the nozzle and the platform may collide with each other during printing. To avoid this issue, the receiving sub-platform can be pre-printed to achieve the printing of the cantilever structure model of the spiral tube. As shown in Fig. 16(a), when the platform is inclined, the nozzle module easily collides with the printing platform, and a hollow thin-wall structure may be selected for constructing the print receiving sub-platform, thereby greatly reducing the material consumed by the sub-platform.

The 5-axis dynamic slicing print freedom is improved compared to the 3D printing, but the printer is less rigid. With the development of science and technology, the rigidity and accuracy of hardware platforms will continue to increase. If a large-section cantilever structure is printed, due to limitations of the self-extruding diameter of the nozzle, a single-layer printing cannot achieve the layer thickness requirement at each slice position for a larger spacing layer. Therefore, it is necessary to decompose the large-pitched slice layer into many sub-slice layers to increase the density between the large-scale layers at the print slice layer. Because the complexity level and computation time of the algorithm are much higher than the 5-axis dynamic slicing algorithm mentioned above, the layer-by-layer processing for large gap layers requires repeated iterative calculations to further increase the complexity of the algorithm. The 5-axis dynamic printing method for large sections needs further study, with a significant impact in the research for the printing of large-scale cantilever structures using 5-axis printing platforms.

4. Conclusion

The 5-axis dynamic manufacturing is a huge breakthrough compared with the conventional 3D printing, farewell to single layer-by-layer stacking manufacturing form and determined by the control

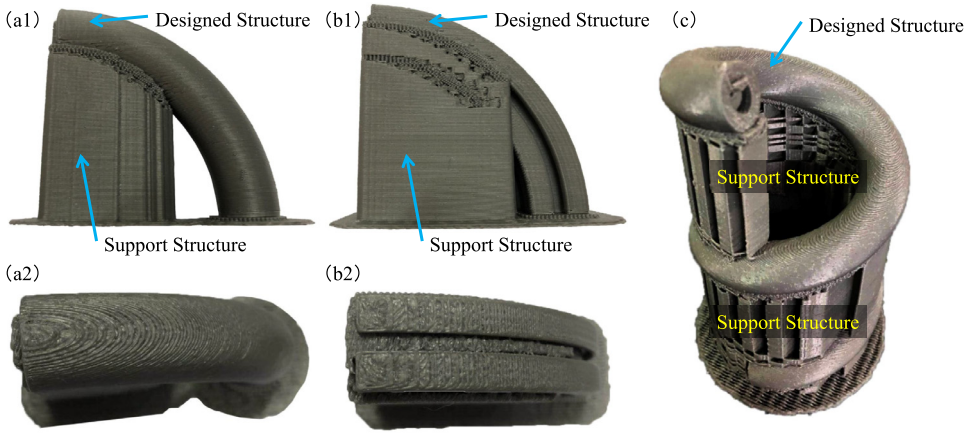

Fig. 13. Cantilever structure model 3D printing effect chart.

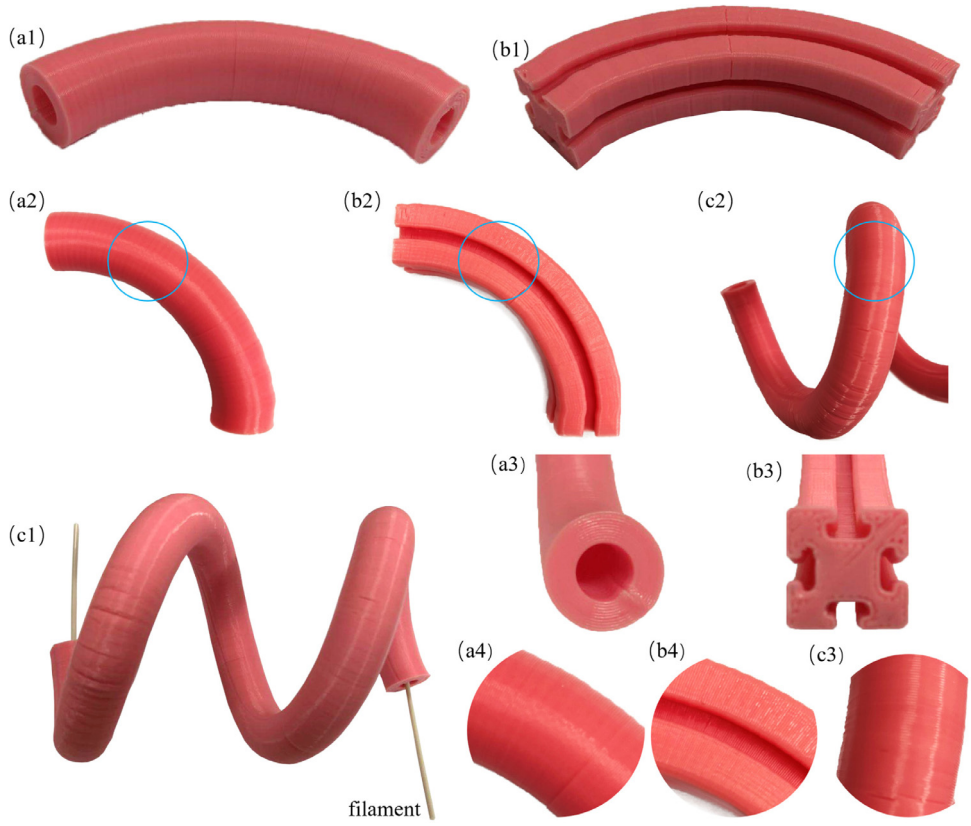

Fig. 14. Cantilever structure model 5-axis dynamic printing surface contour renderings.

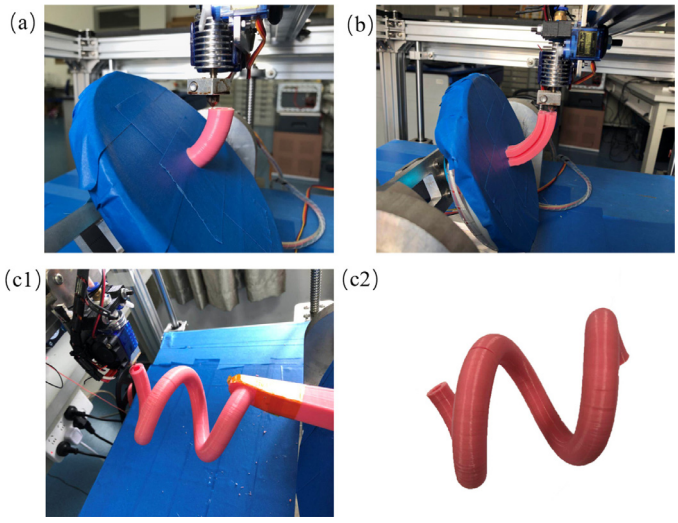

Fig. 15. Cantilever structure model printing.

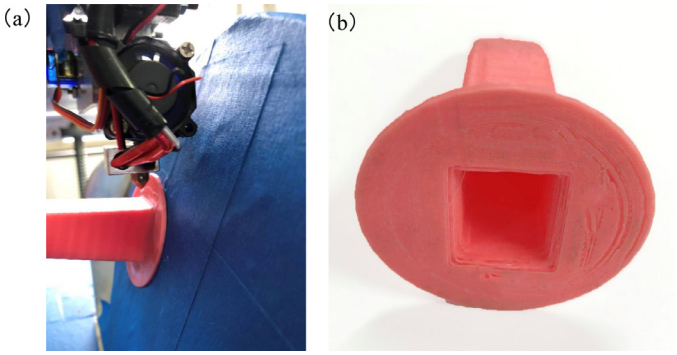

Fig. 16. Sprayer collision diagram and receiving sub-platform.

parameters of the 5-axis dynamic slice through the skeleton extraction of the model. In the 5-axis dynamic manufacturing process, the printed material stacking direction is always along the tangent direction of the model skeleton, so that the model can be easily printed with NSMP.

(1) The comparison of model slicing time and computer memory occupied using different algorithms between conventional 3D printing and 5-axis dynamic printing highlights that for the 5-axis dynamic printing the slicing time increases of about 24.14%–131.98%, and about 15.34%–123.82% the file memory occupied.
(2) The comparison of printing materials and time shows that the 5-axis dynamic printing can save 30.62%–60.61% materials and 32.35%–48.87% time compared to conventional 3D printing. Moreover, the printing materials consumption and efficiency of printed overhang components of the proposed method significantly improved compared to the normal 3D printing. Also, 5-axis dynamic printing never requires post-processing for removing the support structure.
(3) The increased time for the 5-axis dynamic slicing of cantilever model is much lower than the saved printing time compared to the normal 3D printing, and the cost of file memory occupied is much lower than the cost of filament material and manual post-processing.
(4) The staircase effect on the 5-axis dynamic printed parts can be reduced by stacking fused filaments in the direction of the model center skeleton.
For the printing of hollow, slot or spiral-shaped structures, the 5-axis dynamic printing can completely solve the problem of removal of the internal support that conventional FDM 3D printing cannot afford. The 5-axis dynamic manufacturing method reduces the

printing time and the filament consumables during the process of printing the cantilever structure compared to the ordinary 3D printing and avoids the post-treatment process of removing the support, thereby further improving the flexibility, convenience, and economy of the FDM manufacturing process.

Acknowledgements

Thanks to Professor Hu and Professor Zhang for their guidance; the authors acknowledge funding support from the National Natural Science Foundation of China (grant nos. 5177532 and 51375292). The research was supported by the fund of Austrian-Chinese Cooperative R&D Projects and the Shanghai Key Laboratory of Intelligent Manufacturing and Robotics (grant no. ZK1304). The project has been accepted by the Shanghai Aerospace Systems Engineering Institute for the development of a 5-axis motion platform for rapid prototyping of composite materials.

Supplementary materials

Supplementary material associated with this article can be found, in the online version, at doi:10.1016/j.rcim.2019.01.007.

References

[1] Hull C.W., Apparatus for production of three-dimensional objects by stereolithography: U.S. Patent 4575330 1986-3-11.
[2] J.A. Lewis, B.Y. Ahn, Device fabrication: three-dimensional printed electronics, Nature 518 (7537) (2015) 42.
[3] A.S. Arico, P. Bruce, B. Scrosati, et al., Nanostructured materials for advanced energy conversion and storage devices, Nat. Mater. 4 (5) (2005) 366.
[4] A. Goyanes, F. Fina, A. Martorana, et al., Development of modified release 3D printed tablets (printlets) with pharmaceutical excipients using additive manufacturing, Int. J. Pharm. 527 (1–2) (2017) 21–30.
[5] M.S. Mannoor, Z. Jiang, T. James, et al., 3D printed bionic ears, Nano Lett. 13 (6) (2013) 2634–2639.
[6] L. Jonušauskas, D. Gailevičius, L. Mikoliūnaitė, et al., Optically clear and resilient free-form μ-optics 3D-printed via ultrafast laser lithography, Materials 10 (1) (2017) 12.
[7] Y.W.D. Tay, B. Panda, S.C. Paul, et al., 3D printing trends in building and construction industry: a review, Virtual Phys. Prototyp. 12 (3) (2017) 261–276.
[8] W.C. Huang, K.P. Chang, P.H. Wu, et al., 3D printing optical engine for controlling material microstructure, Phys. Procedia 83 (2016) 847–853.
[9] X. Wang, M. Jiang, Z. Zhou, et al., 3D printing of polymer matrix composites: a review and prospective, Composites Part B: Eng. 110 (2017) 442–458.
[10] E. Canessa, C. Fonda, M. Zennaro, et al., Low-cost 3D printing for science, education and sustainable development, Low-Cost 3D Printing, (2013) 11.
[11] H. Zhao, Y. He, J. Fu, et al., Inclined layer printing for fused deposition modeling without assisted supporting structure, Robot. Comput.-Integr. Manuf. 51 (2018) 1–13.
[12] R. Wu, H. Peng, F. Guimbretière, et al., Printing arbitrary meshes with a 5DOF wireframe printer, ACM Trans. Graph. 35 (4) (2016) 101.
[13] K. Lee, H. Jee, Slicing algorithms for multi-axis 3-D metal printing of overhangs, J. Mech. Sci. Technol. 29 (12) (2015) 5139–5144.
[14] S. Keating, N. Oxman, Compound fabrication: a multi-functional robotic platform for digital design and fabrication, Robot. Comput.-Integr. Manuf. 29 (6) (2013) 439–448.
[15] W. Lee, C. Wei, S.C. Chung, Development of a hybrid rapid prototyping system using low-cost fused deposition modeling and five-axis machining, J. Mater. Process. Technol. 214 (11) (2014) 2366–2374.
[16] C. Wu, C. Dai, G. Fang, et al., RoboFDM: a robotic system for support-free fabrication using FDM, 2017 IEEE International Conference on Robotics and Automation (ICRA), IEEE, 2017, pp. 1175–1180.
[17] A. Tagliasacchi, H. Zhang, D. Cohen-Or, Curve skeleton extraction from incomplete point cloud, ACM Trans. Graph. 28 (3) (2009) 71.
[18] T. Colding, W. Minicozzi, E. Pedersen, Mean curvature flow, Bull. Am. Math. Soc. 52 (2) (2015) 297–333.
[19] J.F. Hughes, J.D. Foley, Computer Graphics: Principles and Practice, Pearson Education, 2014.
[20] H. Lipson, M. Kurman, Fabricated: The New World of 3D Printing, John Wiley & Sons, 2013.